

Cite this: *Dalton Trans.*, 2024, **53**, 251

Pyrene fluorescence in 2,7-di(4-phenylethynyl)pyrene-bridged bis(alkenylruthenium) complexes†

Franciska S. Gogesch,^a Lea Bauer,^a Florian D. Vollstädt,^a Michael Linseis,^a Laura Senft,^b Ivana Ivanović-Burmazović^b and Rainer F. Winter^{id}*^a

Complexes **PyrDPE-Ru_{Cl}** and **PyrDPE-Ru_{acac}** with a π -extended 2,7-di(4-phenylethynyl)pyrene linker undergo simultaneous one-electron oxidations of their {Ru}-styryl entities. The absence of an intervalence charge-transfer (IVCT) band at intermediate stages, where the mixed-valent, singly oxidized radical cation is present, and spin density confinement to the terminal styryl ruthenium site(s) are tokens of a lack of electronic coupling between the {Ru} entities across the π -conjugated linker. The close similarity of the linker-based $\pi \rightarrow \pi^*$ bands in the complexes and the free ligand and their insensitivity towards oxidations at the terminal sites indicate that the central pyrenyl fluorophore is electronically decoupled from the electron-rich {Ru}-styryl termini. As a consequence, the complexes offer stable pyrene-based fluorescence emissions at 77 K, which are red-shifted from that of the linker.

Received 22nd September 2023,
Accepted 24th November 2023

DOI: 10.1039/d3dt03114d

rsc.li/dalton

Introduction

Bis(alkenylarylene)-bridged diruthenium complexes of the type $\{[Ru]_2(\mu-CH=CH-arylene-CH=CH)\}$ ($\{Ru\} = \{(PR_3)_2Cl(CO)(L)Ru\}$, where $L = PR_3$ or a vacant coordination site, or $\{Ru\} = \{(PR_3)_2(L_2)(CO)Ru\}$ with a bidentate monoanionic carboxylate or β -ketoenolate ligand L_2) are widely studied with respect to bridge *versus* metal contributions to the individual redox processes,^{1,2-5} their polyelectrochromic properties,^{2,3,6-8} and the extent of charge and spin density delocalization in their one-electron oxidized, mixed-valent states.⁹⁻¹¹ As a general trend, bridge contributions to the relevant molecular orbitals (MOs) increase as the π -conjugated linker gets longer. Instructive examples are given by the series arylene = 1,4-phenylene (**1**),^{2,12,13} 4,4'-biphenylene (**2**),^{14,15} stilbene-4,4'-diyl (**3**),¹⁰ 4,7-benzo[2,1,3]-thiadiazole-diyl (**4a**), and bis(4-benzothiazol[2,1,3]-ethyne-7,7'-diyl (**4b**),¹¹ as well as *trans,trans*-distyryl-benzenediyl (**5a**) or 1,4-bis(ethynylphenyl)benzenediyl (**5b**) (see Fig. 1 for structures).^{4,5,16} Several of the linkers employed in these studies are luminescent as the free or TMS-protected alkynes.¹⁷ However, emission from such complexes was only rarely observed.¹⁸ In particular, all complexes in Fig. 1 are non-emissive. According to common wisdom, the appended, electron-rich ruthenium end groups quench the emission from

the π -conjugated linkers by energy or electron transfer, with the concomitant population of non-emissive excited d- or charge-transfer states.^{5,13} The turn-on of ligand-based luminescence on detaching the fluorophore from the metal ion was elegantly used to monitor the formation of catalytically competent species from dormant precatalysts.¹⁹

In this study, we present the two diruthenium complexes **PyrDPE-Ru_{Cl}** and **PyrDPE-Ru_{acac}** with a π -extended 2,7-bis[(4-vinylphenyl)ethynyl]pyrene bridging ligand. In these complexes, the large extension of the linker electronically decouples its pyrenylene core from the terminally appended styryl

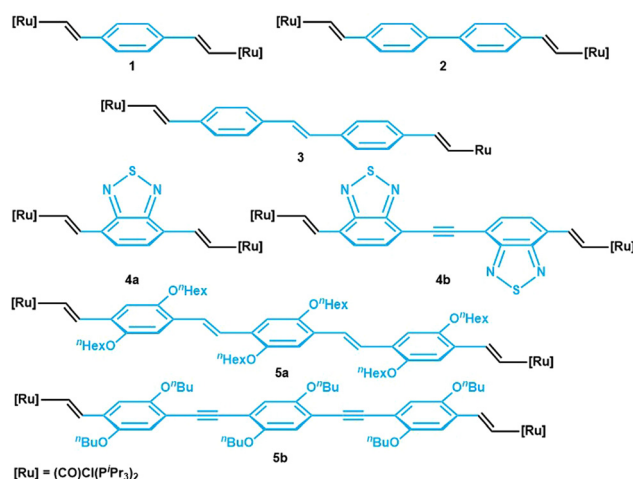


Fig. 1 Series of previously reported ruthenium complexes with π -conjugated linkers of different length.

^aFachbereich Chemie, Universität Konstanz, Universitätsstraße 10, 78457 Konstanz, Germany. E-mail: rainer.winter@uni-konstanz.de

^bFachbereich Chemie, Ludwig-Maximilians-Universität München, Butenandtstraße 5-13, Haus D, 81377 München, Germany

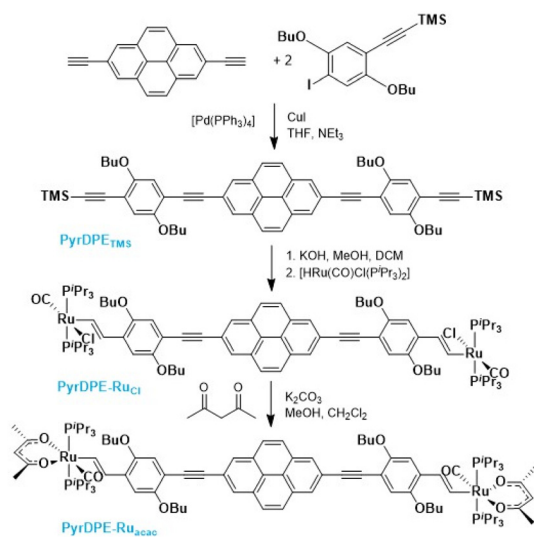
† Electronic supplementary information (ESI) available. See DOI: <https://doi.org/10.1039/d3dt03114d>

ruthenium redox sites. Electronic excitation into the $\pi \rightarrow \pi^*$ bands of the linker provides stable, ligand-based fluorescence emission from the pristine complexes at 77 K.

Results and discussion

Scheme 1 summarizes the synthetic routes to complexes **PyrDPE-Ru_{Cl}** and **PyrDPE-Ru_{acac}** and their ligand precursors along with their chemical structures. The synthesis of the new dialkyne **PyrDPE_{TMS}** started from 2,7-diethynylpyrene, which was synthesized according to a published procedure.^{20,21} Coupling with two equivalents (equiv.) of the trimethylsilyl-protected monoalkynyl building block 2,5-dibutoxy-4-iodo-1-(trimethylsilylethynyl)benzene²² under Sonogashira conditions provided **PyrDPE_{TMS}** in a yield of 39%. Deprotection to the free dialkyne **PyrDPE_H** and its treatment with two equiv. of [HRu(CO)Cl(P^tPr₃)₂] resulted in the regio- and stereoselective insertion of the terminal ethynyl functionalities into the Ru–H bond of the hydride complex²³ to afford **PyrDPE-Ru_{Cl}**. The latter was isolated as a red solid in a yield of 47%. **PyrDPE-Ru_{acac}** was obtained in 59% yield by substitution of the terminal chloro ligands with *in situ* generated acetylacetonate (Scheme 1).

NMR spectroscopy and mass spectrometry (MS) characterization data are collected in the ESI.† The corresponding spectra are shown as Fig. S2–S12 of the ESI.† Characteristic spectroscopic features are the singlet resonance in their ³¹P{¹H} NMR spectra with chemical shifts δ of 38.8 ppm for **PyrDPE-Ru_{Cl}** and 35.6 ppm for **PyrDPE-Ru_{acac}**, and the two sets of resonances at $\delta = 9.28$ and 7.01 ppm, or $\delta = 9.54$ and 7.47 ppm, for the α and β vinyl protons of **PyrDPE-Ru_{Cl}** and **PyrDPE-Ru_{acac}** (³*J*_{HH} = 13.3 or 16.6 Hz), respectively. The resonances of the β vinyl protons are split into a triplet-of-doublet by *J*_{PH} couplings of *ca.* 2 Hz to the phosphorus nuclei of the P^tPr₃ ligands. In



Scheme 1 Synthesis and chemical structures of complexes **PyrDPE-Ru_{Cl}** and **PyrDPE-Ru_{acac}** and the ligand precursors.

¹³C NMR spectra, the CO resonance of the carbonyl ligands is observed as a triplet at $\delta = 203.6$ ppm for **PyrDPE-Ru_{Cl}**, and at $\delta = 210.1$ ppm for **PyrDPE-Ru_{acac}** with ²*J*_{CP} = 13.4 or 15.4 Hz.⁷ Appending the electron-rich ruthenium moieties causes a downfield shift of the closer alkynyl C atom by *ca.* 2.5 ppm, and downfield shifts of *ca.* 1.5 ppm for the other alkynyl C and the *ipso* pyrenyl C atoms, but has only minor effects on the other carbon atoms of the pyrenyl core.

Cyclic and square-wave voltammograms were recorded in the CH₂Cl₂/0.1 M ⁿBu₄N⁺ PF₆[−] electrolyte in order to explore the redox properties of the two complexes and compare them to those of their protected dialkyne precursor **PyrDPE_{TMS}**. In their cyclic voltammograms, **PyrDPE-Ru_{Cl}** and **PyrDPE-Ru_{acac}** display two widely spaced redox-waves (Fig. 2 and Fig. S14 and S15 of the ESI†). The first wave constitutes a chemically and electrochemically reversible redox couple. The second process is chemically irreversible (or nearly so) at low sweep rates *v*, but attains at least partial chemical reversibility at higher *v*. This allowed us to determine the half-wave potentials *E*_{1/2} for both oxidations from the average potentials of the anodic forward and cathodic reverse peaks. Comparison shows that coordinative saturation of the {Ru} end-groups decreases the half-wave potential of the first redox couple by 196 mV, but has a smaller effect of 48 mV on the second oxidation (Table 1).

Even the second wave is however found at less positive potential than the first oxidation of the TMS-protected ligand precursor **PyrDPE_{TMS}**, which shows only a single, partially reversible anodic wave at *E*_{1/2} = 840 mV (see Fig. S13 of the ESI†).

As will be detailed later, the first wave of complexes **PyrDPE-Ru_{Cl}** and **PyrDPE-Ru_{acac}** corresponds to a two-electron

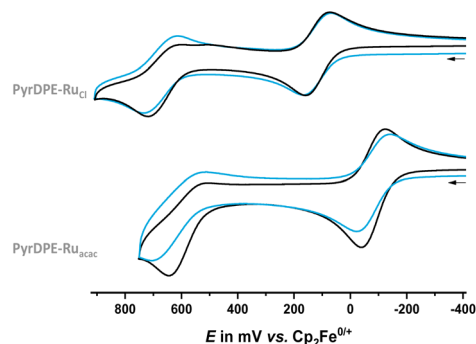


Fig. 2 Cyclic voltammograms of **PyrDPE-Ru_{Cl}** (top) and **PyrDPE-Ru_{acac}** (bottom) in CH₂Cl₂/ⁿBu₄N⁺ PF₆[−] (0.1 M) at *T* = 293 K at a scan rate *v* of 100 (black) and 1000 mV s^{−1} (blue).

Table 1 Electrochemical data for **PyrDPE-Ru_{Cl}**, **PyrDPE-Ru_{acac}** and precursor **PyrDPE_{TMS}**, measured in CH₂Cl₂/ⁿBu₄N⁺ PF₆[−]. Potentials are reported against the ferrocene/ferrocenium couple at *E*_{1/2} = 0 mV

	<i>E</i> _{1/2} ^{0/2+} [mV]	<i>E</i> _{1/2} ^{2+/4+} [mV]	$\Delta E_{1/2}$ [mV]
PyrDPE_{TMS}	840	n.a.	n.a.
PyrDPE-Ru_{Cl}	126	678	552
PyrDPE-Ru_{acac}	−70	630	700



process which involves the electron-rich styryl ruthenium entities. The same also seems to apply to the second oxidation as inferred from the similar heights of the anodic forward peak and probably also to protected alkyne **PyrDPE_{TMS}**, where the outer, electron-rich phenyl rings constitute the most likely redox sites.²⁴ Sizable shifts of oxidation waves to lower potentials and enhanced chemical stabilities of the electrogenerated oxidized forms as compared to the free ligands are common assets of mononuclear ruthenium styryl and arylene-bridged diruthenium complexes.^{2,6,10,25} The present complexes thus complement the series of 1,4-phenylene-,² 4,4'-biphenylene-,¹⁵ 4,4'-stilbene-4,4'-diyl-¹⁰ and distyrylbenzenediyl- or 1,4-bis(ethynylphenyl)benzenediyl-bridged¹⁶ diruthenium complexes with the insertion of a 2,7-diethynylpyrene-diyl unit into the π -conjugated linker. Within this series, the half-wave potential splitting $\Delta E_{1/2}$ between the two consecutive oxidations of the alkenyl ruthenium entities decreases from 250 to 100 mV, and then 49 or 40 mV, until it completely vanishes in the present complexes.

In order to experimentally probe the hypothesis of alkenyl ruthenium-based oxidations and the two-electron nature of the first redox wave, we monitored the oxidation-induced changes in the UV/Vis/NIR and IR/NIR spectra by chemical oxidation and by spectroelectrochemistry (SEC), employing an optically transparent thin-layer electrolysis (OTTLE) cell.²⁶ Redox titrations with simultaneous spectroscopic monitoring and comparison with the SEC results (Fig. S18, S19, S22 and S23 of the ESI[†]) showed that two equivalents of the chemical oxidant acetylferrocenium hexafluoroantimonate ($E_{1/2}^{0/+} = 0.27$ V) or 1,1'-diacetylferrocenium hexafluoroantimonate ($E_{1/2}^{0/+} = 0.49$ V)²⁷ are required in order to achieve full conversion of the neutral complexes to their oxidized forms generated after electrolysis at a potential past the first redox wave (see Fig. S16 and S17 of the ESI[†]). This proves the two-electron nature of the first and, by inference from the identical peak currents, also the second redox wave of the complexes.

Fig. 3 and 4 compare the mid-IR and UV/Vis/NIR spectra of the neutral and the dicationic complexes. Upon oxidation, the CO stretching vibration of the Ru-bonded carbonyl ligands blue-shifts by 44 (1915 \rightarrow 1959 cm^{-1}) or 54 cm^{-1} (1900 \rightarrow 1954 cm^{-1}). The magnitude of this shift is in the expected range for the full oxidation of a styryl {Ru} unit in a diruthenium divinylarylene complex, *i.e.* on the conversion of neutral divinylarylene-bridged diruthenium complexes to their

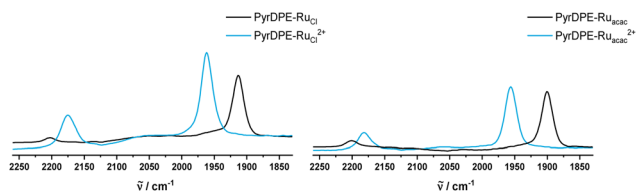


Fig. 3 IR spectra of **PyrDPE-Ru_{Cl}** and **PyrDPE-Ru_{Cl}²⁺** (left) and **PyrDPE-Ru_{acac}** and **PyrDPE-Ru_{acac}²⁺** in CH_2Cl_2 . The dications were generated by chemical oxidation (see text).

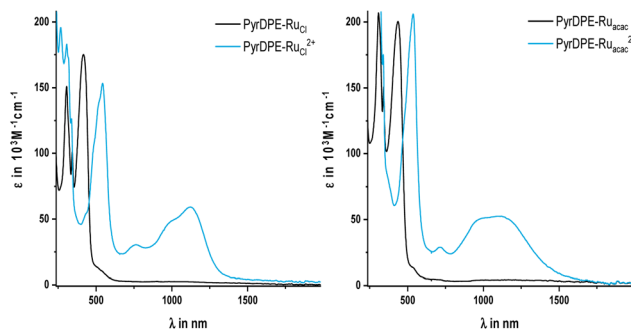


Fig. 4 UV/Vis/NIR spectra of chemically oxidized **PyrDPE-Ru_{Cl}** and **PyrDPE-Ru_{Cl}²⁺** (left) and **PyrDPE-Ru_{acac}** and **PyrDPE-Ru_{acac}²⁺** (right), measured in CH_2Cl_2 .

dications.^{2,6,10,15,16,25} The sizable Ru(CO) band shift also confirms that the redox processes are biased towards the termini rather than the central pyrenyl part of the linker. The larger magnitude of the CO band shift in **PyrDPE-Ru_{acac}** agrees with the notion, that metal contributions to the redox orbitals increase as the {Ru} termini are rendered more electron-rich.

During oxidation, the C \equiv C stretching vibration gains in intensity and red-shifts from 2202 to 2175 cm^{-1} for **PyrDPE-Ru_{Cl}**, or to 2181 cm^{-1} for **PyrDPE-Ru_{acac}**. The observed intensity increase is also in line with an enhanced polarity at the alkenyl linkages concomitant with the oxidation at the two termini.

Just like the ligand precursor **PyrDPE_{TMS}**, the neutral complexes feature three prominent $\pi \rightarrow \pi^*$ absorption bands in their UV/Vis spectra. The latter are located at 416 or 435 nm (ϵ *ca.* 180 000 $\text{M}^{-1} \text{cm}^{-1}$), 340 nm (ϵ *ca.* 125 000 to 175 000 $\text{M}^{-1} \text{cm}^{-1}$), and 305 nm (ϵ *ca.* 200 000 $\text{M}^{-1} \text{cm}^{-1}$). Attachment of the ruthenium termini does not affect the band pattern, but causes a distinct red-shift of the band at the lowest energy from 379 nm in **PyrDPE_{TMS}** to 416 or 435 nm in **PyrDPE-Ru_{Cl}** or **PyrDPE-Ru_{acac}**, whereas it has no such effect on other two. As the oxidation proceeds, the band at the lowest energy bleaches and is replaced by a new, further red-shifted feature of similar intensity (Fig. 4). In contrast, the UV bands experience only minor changes, apart from some intensity increase for **PyrDPE-Ru_{Cl}**. Oxidation of the outer styryl ruthenium entities also causes the emergence of a vibrationally structured NIR band, which extends from 900 to 1600 nm, and of a weaker, separate feature at *ca.* 750 nm (see also Fig. S22 and S23 of the ESI[†]). During no stage of the SEC experiments we were able to detect any additional spectroscopic features that would be assignable to the intermittently formed, one-electron oxidized radical cation. The same also holds for the Ru(CO) bands in the IR, where spectra recorded at intermediate stages or after adding one equiv. of the chemical oxidant have profiles that match with those of mixtures of the neutral and dicationic forms of the complexes. Even when both termini oxidize at the same potential and when the comproportionation constant K_c (eqn (1)) assumes a value of 1, the mixed-valent radical cation must be the dominant species in solution near



the electrode surface after passage of one equiv. of charge or after treatment of the neutral complexes with one equiv. of oxidant. The lack of any spectroscopic signatures specific of the radical cations thus characterizes **PyrDPE-Ru_{Cl}^{•+}** and **PyrDPE-Ru_{acac}^{•+}** as mixed-valent systems of Class I according to the scheme of Robin and Day²⁸ with non-interacting, mutually insulated redox sites. The present complexes thus continue the series of bis(alkenylarylene)-bridged diruthenium complexes, where the extent of electronic coupling in the mixed-valent state is seen to taper off with increasing length of the π -conjugated linker, *i.e.* from intrinsic delocalization in 1,4-phenylene-bridged **1^{•+}**,² to partial charge localization in the 4,4'-biphenylene- and stilbenyl-4,4'-diyl-bridged complexes **2^{•+}** and **3^{•+}** and in **4a,b^{•+}**,^{10,15} very weak delocalization in one-electron oxidized **5a^{•+}** and **5b^{•+}** (Fig. 1), and finally to charge localization in the present complexes.

$$K_c = \exp\left(\frac{F}{RT} (E_{1/2}^{+/2+} - E_{1/2}^{0/+})\right) = \exp\left(\frac{F}{RT} (\Delta E_{1/2})\right) \quad (1)$$

Confinement of the oxidation to the two termini and the lack of electronic coupling between them are also indicated by EPR spectroscopy. EPR spectra were recorded after adding 0.2 equiv. of ferrocenium hexafluorophosphate (**PyrDPE-Ru_{acac}**) or acetylferrocenium hexafluoroantimonate (**PyrDPE-Ru_{Cl}**), or 2.1 equiv. of acetylferrocenium hexafluoroantimonate as suitable oxidants to solutions of **PyrDPE-Ru_{Cl}** or **PyrDPE-Ru_{acac}**. Adding only 0.2 equiv. of the oxidant to the neutral complexes guarantees that the singly oxidized radical cations are the dominating EPR active species in solution. So generated samples of **PyrDPE-Ru_{Cl}^{•+}** provided an isotropic EPR signal at $g_{\text{iso}} = 2.017$ with detectable hyperfine splittings (hfs) to two ³¹P nuclei (9.1 G) and one ^{99/101}Ru nucleus (7.5 G). Nearly identical spectra were obtained from samples of two-electron oxidized **PyrDPE-Ru_{Cl}²⁺** (Fig. 5). This confirms that the unpaired spin density is confined to the {Ru}-CH≡CH-phenyl sites and localized on only a single ruthenium styryl entity in **PyrDPE-Ru_{Cl}^{•+}**. No resolved hfs can be discerned for samples of six-coordinated **PyrDPE-Ru_{acac}^{•+/2+}**, which give an isotropic EPR signal at a slightly higher g value (see Fig. S24–S26 of the ESI† and Table 2), concomitant with larger Ru contributions to the SOMO. The intense EPR signals of the dications likewise agree

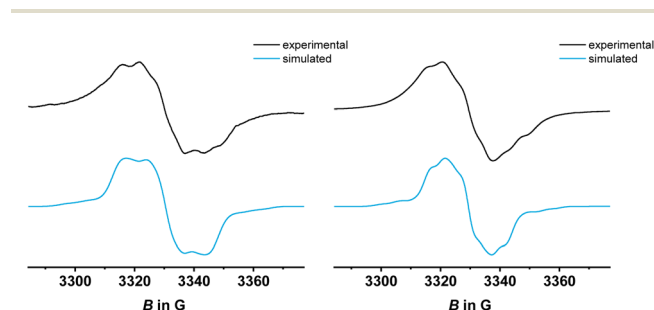


Fig. 5 Comparison of experimental and simulated EPR spectra of chemically generated **PyrDPE-Ru_{Cl}^{•+}** (left) and **PyrDPE-Ru_{Cl}²⁺** (right), measured in CH₂Cl₂ at r.t.

Table 2 EPR spectroscopic data for **PyrDPE-Ru_{Cl}^{•+/2+}** and **PyrDPE-Ru_{acac}^{•+/2+}**; hyperfine coupling constants A are given in Gauss^a

	g_{iso}	A (³¹ P)	A (^{99/101} Ru)	A (¹ H) ^b
PyrDPE-Ru_{Cl}^{•+}	2.017	9.1 (2)	7.5 (1)	4.8 (1), 4.1 (1)
PyrDPE-Ru_{Cl}²⁺	2.017	7.3 (2)	6.8 (1)	4.1 (1), 3.9 (1)
PyrDPE-Ru_{acac}^{•+/2+}	2.023	—	—	—

^a Measured at r.t. in CH₂Cl₂. ^b hfs to the α and β vinyl protons.

with the notion of a lack of electronic coupling between the terminal redox sites, so that they act as independent spin centers.

(TD)-DFT calculations on slightly truncated PMe₃ models of complexes **PyrDPE-Ru_{Cl}** and **PyrDPE-Ru_{acac}** at the pbe1pbe/6-31G(d)/PCM (ClCH₂-CH₂Cl) level of theory²⁹ are fully consistent with our experimental findings. As can be seen in Fig. 6, the occupied frontier MOs HOMO and HOMO-1 represent the in- and out-of-phase combinations of MOs that are constituted by the {Ru}-styryl entities and the alkynyl linkers. In the absence of electronic coupling, one would expect that the HOMO and HOMO-1 are degenerate. However, small admixtures of pyrene-based π MOs with different nodal properties and energies lift their degeneracy and cause a small energy difference of 0.14 or 0.13 eV between them. The LUMO and LUMO+1 in turn extend over the entire 4,9-di(4-phenylethynyl) pyrene linker or are confined to the pyrenediyl entity.

TD-DFT calculations provide further insight into the nature of the electronic excitations. Computed transitions, contour diagrams of the involved donor and acceptor orbitals, and the corresponding electron density difference maps (EDDMs) as well as comparisons between experimental and computed spectra of the neutral and dicationic forms of the complexes are shown as Fig. S34 to S44 of the ESI.† Exciting the neutral complexes into the HOMO \rightarrow LUMO band transfers electron density from the periphery to the inner pyrenediyl segment of the linker. The latter excitation corresponds to the most red-

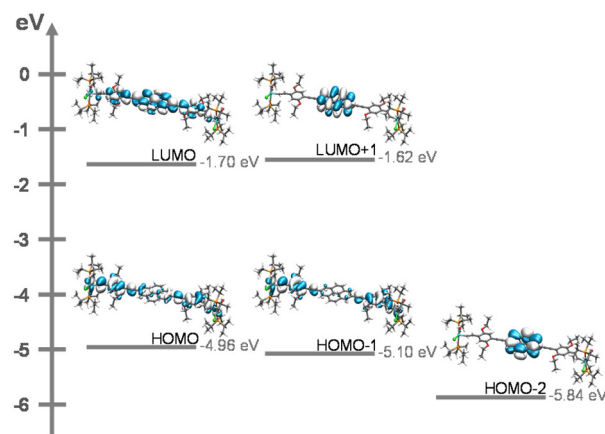


Fig. 6 Contour diagrams of HOMO-2 to LUMO+1 of the PMe₃ model of complex **PyrDPE-Ru_{Cl}**.



shifted, intense Vis band at *ca.* 420 nm of the complexes. In contrast, the UV bands result from $\pi \rightarrow \pi^*$ excitations between orbitals that extend over the entire linker or are confined to either the outer styryl ruthenium entities or the pyrenediyl unit and do not involve charge transfer. The lack of {Ru} contributions to the ligand $\pi \rightarrow \pi^*$ excitations also explains why these bands show only minor shifts from **PyrDPE_{TMS}** and during twofold oxidation.

For the dicationic forms of the complexes, the closed-shell singlet (S), the open-shell singlet (OSS), and triplet (T) states need to be considered. Our calculations place the T state by 62.7 or 54.3 kJ mol⁻¹ below the S state, and by 5.1 or 59.8 kJ mol⁻¹ below the OSS state. As Fig. S36 and S41 of the ESI† show, computed spectra for the T and the OSS states of **PyrDPE-Ru_{Cl}²⁺** as well as the T state of **PyrDPE-Ru_{acac}²⁺** reproduce the experimentally observed UV/Vis/NIR spectroscopic features very well. The intense NIR band of the dicationic complexes is due to excitations between MOs that are confined to the {Ru} styryl entities and involve the transfer of electron density from the donor-substituted phenyl rings (**PyrDPE-Ru_{Cl}**) or the acac coligands (**PyrDPE-Ru_{acac}**) to the {Ru}-CH=CH acceptor units (see Fig. S38, S39 and S43 of the ESI† for the contributing MOs and the EDDMs of the individual transitions). The prominent Vis band at *ca.* 500 nm likewise involves charge transfer from the ethynylphenylene linkers to the vinyl ruthenium tags.

Given these properties, we mused that electronically decoupling the linker, and particularly the central pyrene fluorophore, from MOs with metal contributions may attenuate the efficacy of reductive emission quenching of pyrene-centered excited states. This prompted us to also study the emissive properties of the two complexes and compare them to those of their dialkyne precursor **PyrDPE_{TMS}**. In a glassy methylcyclohexane matrix at 77 K, excitation into any of the $\pi \rightarrow \pi^*$ absorption bands indeed triggers blue fluorescence emission from **PyrDPE-Ru_{Cl}** and **PyrDPE-Ru_{acac}** with a main peak at 460 or 475 nm (see Fig. 7 and Table 3) and an emission envelope that is highly reminiscent of that of pyrenes. While being red-shifted and less-well resolved, the complexes' emissions closely resemble that of **PyrDPE_{TMS}** ($\lambda_{\text{max,Fl}}$ = 427 nm, fluorescence quantum yield Φ_{Fl} = 0.17 at r.t.). We also note that the fluorescence lifetimes of the complexes of 45.3 or 45.1 ns, respectively, are smaller than that of 78.5 ns for **PyrDPE_{TMS}** at *T* = 77 K (similar trends pertain to additional, more short-lived contributors, see Table 3). Excitation spectra recorded at the fluorescence maxima of **PyrDPE-Ru_{Cl}** and **PyrDPE-Ru_{acac}** at *T* = 77 K match with the respective absorption spectra, but with enhanced resolution of the individual peaks. The resolved vibrational progression of *ca.* 430 cm⁻¹ is likewise typical of pyrenes³⁰ and resembles that in **PyrDPE_{TMS}**. The excitation spectra of **PyrDPE_{TMS}** and **PyrDPE-Ru_{acac}** at 77 K display a red-shift of the 0 → 0 peak when compared to the absorption in fluid solution at r.t. We attribute this to lower degrees of conformational freedom and higher proportions of conformers with smaller torsions around the C-C linkages of the π -conjugated backbone at this temperature, which enhances

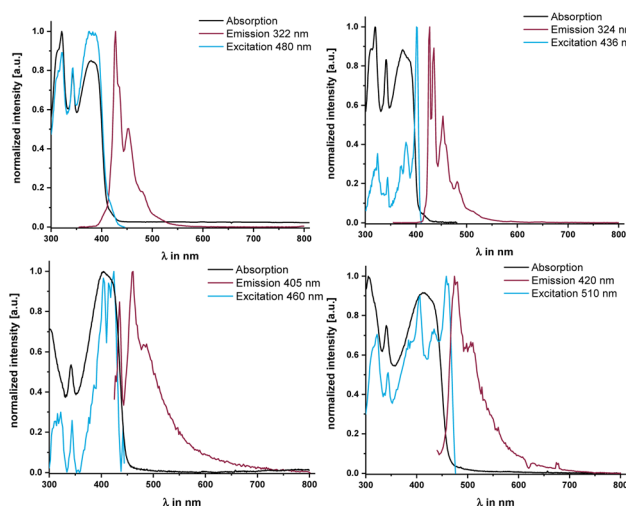


Fig. 7 Emission spectra of **PyrDPE_{TMS}** in CH_2Cl_2 solution at r.t. (top left) and in methylcyclohexane solution at 77 K (top right), and of **PyrDPE-Ru_{Cl}** (bottom left) and **PyrDPE-Ru_{acac}** (bottom right) in methylcyclohexane solution at 77 K.

Table 3 Photophysical data of **PyrDPE_{TMS}**, **PyrDPE-Ru_{Cl}** and **PyrDPE-Ru_{acac}** in a glassy methylcyclohexane matrix at 77 K

	$\lambda_{\text{max,Fl}}$ (nm) (Stokes shift cm ⁻¹)	τ_{Fl} ^a (ns) (contribution in %)
PyrDPE_{TMS}	427 (1519)	78.5 (95), 1.6 (5)
PyrDPE-Ru_{Cl}	460 (596)	45.3 (33), 9.3 (31), 0.6 (36)
PyrDPE-Ru_{acac}	475 (737)	45.1 (26), 5.0 (33), 0.7 (41)

^a Relative intensities in %.

π -conjugation. Such effects were already noted for (oligo) phenylenevinylenes.³¹

PyrDPE-Ru_{Cl} and **PyrDPE-Ru_{acac}** however proved to be unstable towards irradiation at r.t. in fluid CH_2Cl_2 solution. Emission spectra recorded under these conditions showed sizable blue-shifts of the original peaks from their positions at 77 K, when luminescence spectra are recorded in CH_2Cl_2 at r.t. The r.t. emissions resemble that of **PyrDPE_{TMS}** measured under the same conditions closely (see Fig. S27 of the ESI†). Moreover, excitation spectra recorded at the emission maxima and UV/Vis spectra recorded after laser excitation at r.t. do no longer show the characteristic Vis absorption of the complexes at *ca.* 420 nm, but instead a blue-shifted band akin to that of **PyrDPE_{TMS}**. The same spectral changes are observed when a CH_2Cl_2 solution of **PyrDPE-Ru_{Cl}** is irradiated with a LED lamp at a wavelength of 275 nm. The bleaching of the characteristic Vis absorption is accompanied by the loss of the original vinyl -CH=CH- resonances in the ¹H NMR spectrum of a photolyzed solution. Both these findings suggest that the ruthenium-alkenyl bonds are cleaved upon r.t. irradiation. IR and NMR spectra recorded from the photolyzed solution suggest that a complex of the type $[\text{Ru}(\text{CO})_2(\text{P}^i\text{Pr}_3)_2(\text{Cl})(\text{X})]$ with *trans*-



coordinated P^iPr_3 ligands and mutually *cis*-disposed ligands Cl and X is formed, where X is neither the original alkenyl ligand nor H (for further details see Fig. S30–S33 and the accompanying explanations in the ESI†).

In conclusion, we have shown that fluorophores embedded in a π -extended bridging ligand can retain their emissive properties, once they are electronically decoupled from electron-rich metal end groups that normally act as quenchers. This adds luminescence spectroscopy to the toolbox available for probing electron (de)localization over π -extended ligands in such complexes.

Materials and methods

Methods

All syntheses were performed with standard Schlenk techniques under an atmosphere of purified nitrogen with dry, distilled, and degassed solvents. Commercially available starting materials were used as received. 4,9-Diethynylpyrene^{20,21} and 2,5-dibutoxy-4-iodo-1-(trimethylsilylethynyl)benzene²² were prepared according to published literature procedures.

For NMR experiments, 1H NMR (400 MHz), ^{13}C NMR (101 MHz), and ^{31}P NMR (162 MHz) spectra were measured on a Bruker Avance III 400 spectrometer, 1H NMR (600 MHz) and ^{13}C NMR (151 MHz) spectra on a Bruker Avance III 600 spectrometer, and 1H NMR (800 MHz), ^{13}C NMR (202 MHz), and ^{31}P NMR (324 MHz) on a Bruker Avance Neo 800 instrument. NMR data are given as follows: chemical shift (δ in ppm), multiplicity (s, singlet; d, doublet; t, triplet; td, triplet of doublets; vt, virtual triplet; vq, virtual quartet; vsxt, virtual sextet; m, multiplet), integration, coupling constant (Hz). Unequivocal signal assignments were achieved by 2D NMR experiments. The numbering of the nuclei follows that of the chemical structures displayed with the synthesis protocols.

Mass spectra of organic compounds were recorded on a LTQ Orbitrap Velos instrument (Thermo Scientific) with ESI capable of a resolution of at least 60,000 FWHM in CH_2Cl_2 as a solvent. The spectrometer was calibrated with the Pierce LTQ Velos ESI Positive Calibration Solution (Thermo Fisher Scientific) prior to every measurement. Detection was done in the positive ion mode. The observed data were compared to simulated MS patterns. Mass spectra of organometallic compounds were recorded on an UHR-TOF Bruker Daltonik maXis plus ESI-quadrupole time-of-flight (qToF) spectrometer at a minimum resolution of 60,000 FWHM. Detection was performed in positive ion mode with a source voltage of 3.5 kV and a flow rate of 180 $\mu L h^{-1}$. Nitrogen was used as drying gas. For solvent removal, the temperature was set at 180 °C and the temperature of the spray gas was 20 °C. The calibration was done prior to each measurement by direct infusion of low concentrated Agilent ESI-TOF tuning mixture. This gave an *m/z* range of singly charged peaks of up to 2700 Da.

Cyclic voltammetry was performed under an atmosphere of argon. The voltammograms were recorded using a BASi

Epsilon potentiostat and a custom-made air-tight cell as described elsewhere¹¹ with a platinum electrode ($\varnothing = 1.1$ mm, BASi). The platinum electrode was polished before each measurement with diamond pastes (particle sizes 1 μm and 0.25 μm) from Buehler & Wirtz. Spiral-shaped AgCl Pt wires were used as the reference and counter electrode. 0.1 M $^nBu_4N^+ PF_6^-$ in CH_2Cl_2 was used as the supporting electrolyte. The redox potentials were calibrated against the Cp_2Fe/Cp_2Fe^+ redox couple, which was set as 0 mV.

Spectroelectrochemical measurements were conducted in a custom-made OTTLE cell following the design of Hartl *et al.*²⁶ It comprises of Pt-mesh working and counter electrodes and a thin silver wire as a pseudoreference electrode. The electrodes are sandwiched in between two CaF_2 windows of a conventional liquid IR cell. The working electrode was positioned in the center of the spectrometer beam. The required potential was applied by connecting the cell leads to a Wenking POS2 potentiostat by Bank Elektronik-Intelligent Controls GmbH. As supporting electrolyte, a 0.2 M solution of $^nBu_4N^+ PF_6^-$ in 1,2- $C_2H_4Cl_2$ was used. FT-IR spectra were recorded using a Bruker Tensor II FT-IR spectrometer. UV/Vis/NIR spectra were acquired on a TIDAS fiber optic diode-array spectrophotometer (combined MCS UV/NIR and PGS NIR instrumentation) from j&m Analytik AG.

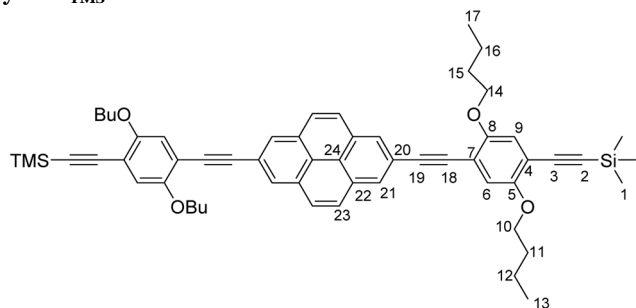
Electron paramagnetic resonance (EPR) studies were conducted on a X-band tabletop spectrometer MiniScope MS 400 by Magnostech GmbH. The complexes were chemically oxidized using ferrocenium hexafluorophosphate ($Cp_2Fe^+ PF_6^-$) or acetylferrocenium hexafluoroantimonate ($AcCp_2Fe^+ SbF_6^-$). Simulation of experimental spectra was performed using the Matlab Easyspin program 'Garlic'.³²

Luminescence spectra and lifetimes as well as quantum yields were measured on a PicoQuant FluoTime 300 spectrometer. The decay lifetimes were adjusted with the FluoFit software. Absolute quantum yields were determined with an integrating sphere within the FluoTime 300 spectrometer.

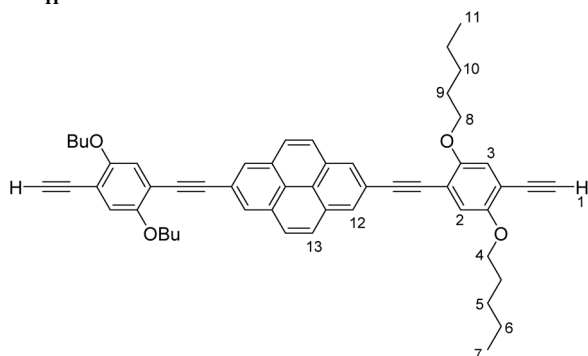
Computational details

The ground state electronic structures of the full models of all compounds were calculated by density functional theory (DFT) methods using the Gaussian 16 program packages.²⁹ Open shell systems were calculated by the unrestricted Kohn–Sham approach (UKS). Geometry optimization followed by vibrational analysis was performed in solvent media. Solvent effects were described by the polarizable continuum model (PCM) with standard parameters for 1,2-dichloroethane.^{33,34} The 6-31G(d) polarized double- ζ basis sets³⁵ were employed for all atoms together with the Perdew, Burke, Ernzerhof exchange and correlation functional (pbe0pbe).^{36,37} The GaussSum program package was used to analyze the results,³⁸ while the visualization of the results was performed with the Avogadro program package.³⁹ Graphical representations of molecular orbitals were generated with the help of GNU Parallel⁴⁰ and plotted using the vmd program package⁴¹ in combination with POV-Ray. Atomic coordinates of the calculated structures are provided in Tables S2–S11 of the ESI.†



PyrDPE_{TMS}

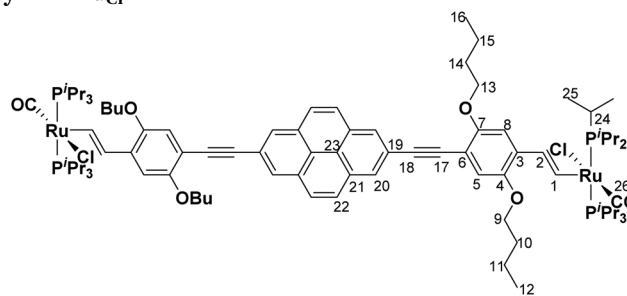
2,7-Diethynylpyrene²⁰ (116 mg, 0.46 mmol, 1.00 equiv.), 2,5-dibutoxy-4-iodo-1-(trimethylsilylethynyl)benzene²² (432 mg, 0.97 mmol, 2.1 equiv.), Pd(PPh₃)₄ (57 mg, 0.05 mmol, 0.05 equiv.) and CuI (4 mg, 0.02 mmol, 0.05 equiv.) were suspended in THF (12 mL) and NEt₃ (3 mL). The resulting mixture was warmed to 60 °C for 12 h. Water was then added and the solution was extracted with CH₂Cl₂. The combined organic phases were dried over MgSO₄. The crude product was washed with *n*-hexane to obtain **PyrDPE_{TMS}** (161 mg, 0.18 mmol) as a yellow solid in 39% yield. ¹H-NMR (CDCl₃, 600 MHz) δ [ppm] = 8.31 (s, 4H, H21), 8.03 (s, 4H, H23), 7.08 (s, 2H, H6), 7.00 (s, 2H, H9), 4.08 (t, ³J_{HH} = 6.4 Hz, 4H, H14), 4.04 (t, ³J_{HH} = 6.4 Hz, 4H, H10), 1.93–1.88 (m, 4H, H15), 1.85–1.80 (m, 4H, H11), 1.69–1.62 (m, 4H, H16), 1.61–1.55 (m, 4H, H12), 1.07 (t, ³J_{HH} = 7.3 Hz, 6H, H17), 1.01 (t, ³J_{HH} = 7.4 Hz, 6H, H13), 0.28 (s, 18H, H1). ¹³C{¹H}-NMR (CDCl₃, 151 MHz) δ [ppm] = 154.4 (s, C5), 153.8 (s, C8), 131.3 (s, C22), 128.8 (s, C21), 127.8 (s, C23), 124.1 (s, C24), 121.5 (s, C20), 117.4 (s, C9), 117.2 (s, C6), 114.3 (s, C7), 114.1 (s, C4), 101.2 (s, C3), 100.4 (s, C2), 95.3 (s, C19), 87.0 (s, C18), 69.5 (s, C10/C14), 69.4 (s, C10/14), 31.6 (s, C11/C15), 31.5 (s, C11/C15), 19.5 (s, C12/C16), 19.4 (s, C12/C16), 14.2 (s, C13/C17), 14.1 (s, C13/C17), 0.1 (s, C1).

PyrDPE_H

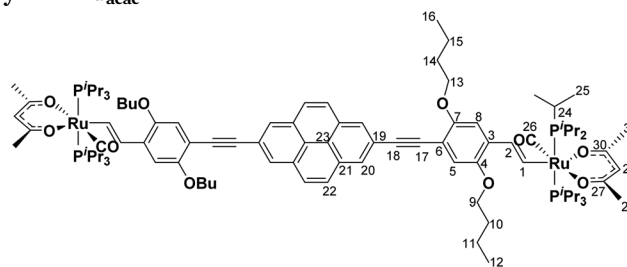
PyrDPE_{TMS} (104 mg, 0.12 mmol, 1.0 eq.) was dissolved in CH₂Cl₂ (10 mL) and MeOH (5 mL). A few drops of water and KOH (5 mg) were added and the resulting solution was stirred for 12 h at room temperature. More water was added and the solution was extracted with CH₂Cl₂. The combined organic phases were dried over MgSO₄ and the solvent was removed under reduced pressure to give **PyrDPE_H** in quantitative yield (90 mg, 0.12 mmol). **PyrDPE_H** was used in the next step without further purification. ¹H-NMR (CDCl₃, 400 MHz) δ

[ppm] = 8.32 (s, 2H, H12), 8.04 (s, 2H, H13), 7.11 (s, 2H, H2), 7.04 (s, 2H, H3), 4.11–4.04 (m, 8H, H8/H4), 3.37 (s, 2H, H1), 1.95–1.87 (m, 4H, H9), 1.87–1.81 (m, 4H, H5), 1.81–1.75 (m, 4H, H10), 1.70–1.61 (m, 4H, H6), 1.09–1.04 (m, 6H, H11), 1.04–0.98 (m, 6H, H7).

PyrDPE-RuCl



PyrDPE_H (87 mg, 0.12 mmol, 1.0 equiv.) was dissolved in CH₂Cl₂ (10 mL) and added dropwise to a solution of [HRu(CO)Cl(PⁱPr₃)₂] (115 mg, 0.24 mmol, 2.0 equiv.) in CH₂Cl₂ (10 mL). The reaction mixture was stirred for 12 h at room temperature. The solvent was removed under reduced pressure and the red solid was washed with MeOH (3 × 10 mL) and with *n*-hexane (3 × 10 mL). **PyrDPE-RuCl** was obtained as a red solid in 47% yield (97 mg, 0.06 mmol). ¹H-NMR (C₆D₆, 600 MHz) δ [ppm] = 9.28 (d, 2H, ³J_{HH} = 13.3 Hz, H1), 8.33 (s, 4H, H20), 7.61 (s, 4H, H22), 7.29 (s, 2H, H5), 7.27 (s, 2H, H8), 7.01 (td, 2H, ³J_{HH} = 13.3 Hz, ⁴J_{HP} = 2.1 Hz, H2), 4.10 (t, 4H, ³J_{HH} = 6.5 Hz, H13), 3.72 (t, 4H, ³J_{HH} = 6.4 Hz, H9), 2.73–2.63 (m, 12H, H24), 1.84–1.78 (m, 4H, H14), 1.73–1.67 (m, 4H, H10), 1.62 (vsxt, 4H, H15), 1.53 (vsxt, 4H, H11), 1.25 (vq, 72H, H25), 0.98 (vq, 12H, H12/16). ¹³C{¹H}-NMR (C₆D₆, 151 MHz) δ [ppm] = 203.6 (t, ²J_{CP} = 13.4 Hz, C26), 155.6 (s, C7), 155.1 (t, ²J_{CP} = 10.8 Hz, C1), 147.9 (s, C4), 131.7 (s, C21), 130.2 (s, C3), 128.9 (s, C2), 128.1 (s, C20), 128.0 (s, C22), 124.3 (s, C23), 122.8 (s, C19), 117.6 (s, C5), 110.2 (s, C8), 109.5 (s, C6), 94.2 (s, C18), 89.3 (s, C17), 69.3 (s, C13), 68.7 (s, C9), 32.0 (s, C10/C14), 31.9 (s, C10/C14), 24.8 (vt, ¹J_{CP} = 9.9 Hz, C24), 20.1 (s, C25), 19.9 (s, C25), 19.8 (s, C11/C15), 19.7 (s, C11/C15), 14.3 (s, C12/C16), 14.2 (s, C12/C16). ³¹P{¹H}-NMR (C₆D₆, 162 MHz) δ [ppm] = 38.8 (s). ESI MS (CH₂Cl₂): 1710.6746 *m/z* ([M]²⁺, calculated 1710.6750 *m/z*). Anal. cacl'd for C₉₀H₁₃₆Cl₂O₆P₄Ru₂: C, 63.18%; H, 8.01%; found: C, 61.69%, H, 8.28%.

PyrDPE-Ru_{acac}

Acetylacetonate (44 mg, 0.45 mL, 0.44 mmol, 15.00 equiv.) and K₂CO₃ in MeOH (15 mL) were warmed for 1 h at 40 °C. The resulting solution was added dropwise to a solution of



PyrDPE-Ru_{Cl} (50 mg, 0.03 mmol, 1.0 equiv.) in CH₂Cl₂ and the resulting mixture was stirred for 1 h at room temperature. The solution was concentrated under reduced pressure and the residue was collected *via* centrifugation. The residue was dissolved in CH₂Cl₂ and insoluble salts were removed by centrifugation. The solvent was removed under reduced pressure and the obtained solid was washed with MeOH (3 × 10 mL). **PyrDPE-Ru_{acac}** was obtained as a yellow solid in 59% yield (31 mg, 0.01 mmol). ¹H-NMR (C₆D₆, 600 MHz) δ [ppm] = 9.54 (d, 2H, ³J_{HH} = 16.6 Hz, H1), 8.32 (s, 4H, H20), 7.61 (s, 4H, H22), 7.51 (s, 2H, H8), 7.47 (td, 2H, ³J_{HH} = 16.6 Hz, ⁴J_{HP} = 1.7 Hz, H2), 7.36 (s, 2H, H5), 5.32 (s, 2H, H29), 4.21 (t, 4H, ³J_{HH} = 6.5 Hz, H13), 3.81 (t, 4H, ³J_{HH} = 6.4 Hz, H9), 2.43–2.34 (m, 12H, H24), 1.90 (s, 6H, H29/H31), 1.86–1.80 (m, 4H, H14), 1.79–1.75 (m, 4H, H10), 1.76 (s, 6H, H29/H31), 1.65–1.55 (m, 8H, H11/H15), 1.35 (vq, 36H, H25), 1.25 (vq, 36H, H25), 0.99 (t, ³J_{HH} = 7.4 Hz, 12H, H12/H16). ¹³C{¹H}-NMR (C₆D₆, 151 MHz) δ [ppm] = 210.0 (t, ²J_{CP} = 15.4 Hz, C26), 188.7 (s, C27/C30), 186.8 (s, C27/C30), 169.3 (t, ²J_{CP} = 11.9 Hz, C1), 155.8 (s, C7), 148.3 (s, C4), 133.2 (s, C3), 131.7 (s, C21), 128.3 (s, C2), 128.1 (s, C20), 127.6 (s, C22), 124.2 (s, C23), 123.0 (s, C19), 118.0 (s, C5), 110.0 (s, C8), 108.6 (s, C6), 100.4 (s, C29), 93.9 (s, C18), 89.8 (s, C17), 69.9 (s, C13), 68.9 (s, C9), 32.2 (s, C10/C14), 32.1 (s, C10/C14), 28.7 (s, C28/30), 28.6 (s, C28/C30), 24.7 (vt, ¹J_{CP} = 8.8 Hz, C24), 20.0 (s, C25), 19.9 (s, C11/C15), 19.8 (s, C11/C15), 19.7 (s, C25), 14.3 (s, C12/C16), 14.2 (s, C12/C16). ³¹P{¹H}-NMR (C₆D₆, 162 MHz) δ [ppm] = 35.6 (s). ESI MS (CH₂Cl₂): 1838.8261 *m/z* ([M]⁺, calculated 1838.8294 *m/z*). Anal. calcd for C₁₀₀H₁₅₀O₁₀P₄Ru₂: C, 65.34%; H, 8.22%; found: C, 64.85%, H, 8.37%.

Conflicts of interest

There are no conflicts to declare.

Acknowledgements

The authors gratefully acknowledge support of this work by the Deutsche Forschungsgemeinschaft (DFG) through Grant Numbers Wi1262/17-1 and INST 40/575-1 FUGG (JUSTUS 2 cluster). We also thank Marcel Geppert and Katharina Deuter for their assistance with the photoluminescence measurements.

References

- (a) J. Maurer, R. F. Winter, B. Sarkar, J. Fiedler and S. Zális, *Chem. Commun.*, 2004, 1900–1901; (b) Y.-P. Ou, J. Zhang, Y. Hu, J. Yin, C. Chi and S. H. Liu, *Dalton Trans.*, 2020, **49**, 16877–16886.
- J. Maurer, B. Sarkar, B. Schwederski, W. Kaim, R. F. Winter and S. Zális, *Organometallics*, 2006, **25**, 3701–3712.
- X. H. Wu, S. Jin, J. H. Liang, Z. Y. Li, G.-A. Yu and S. H. Liu, *Organometallics*, 2009, **28**, 2450–2459.
- Y.-P. Ou, J. Zhang, M. Xu, J. Xia, F. Hartl, J. Yin, G.-A. Yu and S. H. Liu, *Chem. – Asian J.*, 2014, **9**, 1152–1160.
- J. Zhang, Y. Ou, M. Xu, C. Sun, J. Yin, G.-A. Yu and S. H. Liu, *Eur. J. Inorg. Chem.*, 2014, 2941–2951.
- J. Maurer, M. Linseis, B. Sarkar, B. Schwederski, M. Niemeyer, W. Kaim, S. Zalis, C. Anson, M. Zabel and R. F. Winter, *J. Am. Chem. Soc.*, 2008, **130**, 259–268.
- R. Das, M. Linseis, S. M. Schupp, L. Schmidt-Mende and R. F. Winter, *Chem. – Eur. J.*, 2022, **28**, e202104403.
- (a) E. Wuttke, D. Fink, P. Anders, A.-L. Maria Hoyt, W. Polit, M. Linseis and R. F. Winter, *J. Organomet. Chem.*, 2016, **821**, 4–18; (b) Y.-P. Ou, C. Jiang, Di Wu, J. Xia, J. Yin, S. Jin, G.-A. Yu and S. H. Liu, *Organometallics*, 2011, **30**, 5763–5770; (c) W. Y. Man, J.-L. Xia, N. J. Brown, J. D. Farmer, D. S. Yufit, J. A. K. Howard, S. H. Liu and P. J. Low, *Organometallics*, 2011, **30**, 1852–1858; (d) G. Jia, W. F. Wu, R. C. Yeung and H. P. Xia, *J. Organomet. Chem.*, 1997, **539**, 53–59; (e) M. Linseis, R. F. Winter, B. Sarkar, W. Kaim and S. Zális, *Organometallics*, 2008, **27**, 3321–3324; (f) W. Polit, T. Exner, E. Wuttke and R. F. Winter, *BioInorg. React. Mech.*, 2012, **8**, 85–105; (g) O. S. Abdel-Rahman, M. T. Jan, S. Oßwald and R. F. Winter, *J. Organomet. Chem.*, 2017, **849–850**, 98–116; (h) S. Oßwald, S. Breimaier, M. Linseis and R. F. Winter, *Organometallics*, 2017, **36**, 1993–2003.
- (a) P. Mücke, M. Linseis, S. Zális and R. F. Winter, *Inorg. Chim. Acta*, 2011, **374**, 36–50; (b) U. Pfaff, A. Hildebrandt, M. Korb, S. Oßwald, M. Linseis, K. Schreiter, S. Spange, R. F. Winter and H. Lang, *Chem. – Eur. J.*, 2016, **22**, 783–801; (c) W.-X. Liu, F. Yan, S.-L. Qian, J.-Y. Ye, X. Liu, M.-X. Yu, X.-H. Wu, M.-L. Le, Z.-Y. Zhou, S.-H. Liu, P. J. Low and S. Jin, *Eur. J. Inorg. Chem.*, 2017, 5015–5026.
- M. Linseis, S. Zális, M. Zabel and R. F. Winter, *J. Am. Chem. Soc.*, 2012, **134**, 16671–16692.
- N. Rotthowe, J. Zwicker and R. F. Winter, *Organometallics*, 2019, **38**, 2782–2799.
- J. Zhang, C.-F. Sun, X.-H. Wu, M.-X. Zhang, J. Yin, G.-A. Yu and S. H. Liu, *Int. J. Electrochem. Sci.*, 2016, **11**, 7875–7889.
- D.-D. Kong, L.-S. Xue, R. Jang, B. Liu, X.-G. Meng, S. Jin, Y.-P. Ou, X. Hao and S.-H. Liu, *Chem. – Eur. J.*, 2015, **21**, 9895–9904.
- J. Zhang, M.-X. Zhang, C.-F. Sun, M. Xu, F. Hartl, J. Yin, G.-A. Yu, Li Rao and S. H. Liu, *Organometallics*, 2015, **34**, 3967–3978.
- S. Scheerer, N. Rotthowe, O. S. Abdel-Rahman, X. He, S. Rigaut, H. Kvapilová, S. Zális and R. F. Winter, *Inorg. Chem.*, 2015, **54**, 3387–3402.
- F. S. Gogesch, S. Schwab, A. Rehse, M. Linseis, A. Baksi, G. H. Clever and R. F. Winter, *Organometallics*, 2023, **42**, 3085–3098.
- (a) D. A. van Dyke, B. A. Pryor, P. G. Smith and M. R. Topp, *J. Chem. Educ.*, 1998, **75**, 615; (b) P. K. Sahoo, C. Giri, T. S. Haldar, R. Puttreddy, K. Rissanen and P. Mal, *Eur. J. Org. Chem.*, 2016, 1283–1291; (c) K. Žamojć, D. Jacewicz and L. Chmurzyński, *Anal. Lett.*, 2013, **46**, 349–



- 355; (d) H. Maeda, T. Maeda and K. Mizuno, *Molecules*, 2012, **17**, 5108–5125.
- 18 L. Flamigni, A. M. Talarico, B. Ventura, R. Rein and N. Solladié, *Chem. – Eur. J.*, 2006, **12**, 701–712.
- 19 (a) T. Vorfalt, K. J. Wannowius, V. Thiel and H. Plenio, *Chem. – Eur. J.*, 2010, **16**, 12312–12315; (b) P. Kos and H. Plenio, *Chem. – Eur. J.*, 2015, **21**, 1088–1095.
- 20 A. G. Crawford, Z. Liu, I. A. I. Mkhallid, M.-H. Thibault, N. Schwarz, G. Alcaraz, A. Steffen, J. C. Collings, A. S. Batsanov, J. A. K. Howard and T. B. Marder, *Chem. – Eur. J.*, 2012, **18**, 5022–5035.
- 21 M. Inouye, M. S. Itoh and H. Nakazumi, *J. Org. Chem.*, 1999, **64**, 9393–9398.
- 22 A. Harriman, L. J. Mallon, K. J. Elliot, A. Haefele, G. Ulrich and R. Ziessel, *J. Am. Chem. Soc.*, 2009, **37**, 13375–13386.
- 23 (a) H. Werner, M. A. Esteruelas and H. Otto, *Organometallics*, 1986, **5**, 2295–2299; (b) M. A. Esteruelas and H. Werner, *J. Organomet. Chem.*, 1986, **303**, 221–231.
- 24 (a) D.-L. Sun, S. V. Rosokha, S. V. Lindeman and J. K. Kochi, *J. Am. Chem. Soc.*, 2003, **125**, 15950–15963; (b) S. V. Lindeman, S. V. Rosokha, D. Sun and J. K. Kochi, *J. Am. Chem. Soc.*, 2002, **124**, 843–855; (c) S. V. Rosokha, D.-L. Sun and J. K. Kochi, *J. Phys. Chem. A*, 2002, **106**, 2283–2292; (d) D. Sun, S. V. Lindeman, R. Rathore and J. K. Kochi, *J. Chem. Soc., Perkin Trans. 2*, 2001, 1585–1594.
- 25 O. S. Abdel-Rahman, J. Maurer, S. Zálíš and R. F. Winter, *Organometallics*, 2015, **34**, 3611–3628.
- 26 M. Krejčík, M. Daněk and F. Hartl, *J. Electroanal. Chem.*, 1991, **317**, 179–187.
- 27 N. G. Connelly and W. E. Geiger, *Chem. Rev.*, 1996, **96**, 877–910.
- 28 M. B. Robin and P. Day, *Adv. Inorg. Chem. Radiochem.*, 1968, 247–422.
- 29 M. J. Frisch, G. W. Trucks, H. B. Schlegel, G. E. Scuseria, M. A. Robb, J. R. Cheeseman, G. Scalmani, V. Barone, G. A. Petersson, H. Nakatsuji, X. Li, M. Caricato, A. Marenich, J. Bloino, B. G. Janesko, R. Gomperts, B. Mennucci, H. P. Hratchian, J. V. Ortiz, A. F. Izmaylov, J. L. Sonnenberg, D. Williams-Young, F. Ding, F. Lipparini, F. Egidi, J. Goings, B. Peng, A. Petrone, T. Henderson, D. Ranasinghe, V. G. Zakrzewski, J. Gao, N. Rega, G. Zheng, W. Liang, M. Hada, M. Ehara, K. Toyota, R. Fukuda, J. Hasegawa, M. Ishida, T. Nakajima, Y. Honda, O. Kitao, H. Nakai, T. Vreven, K. Throssell, J. J. A. Montgomery, J. E. Peralta, F. Ogliaro, M. Bearpark, J. J. Heyd, E. Brothers, K. N. Kudin, V. N. Staroverov, T. Keith, R. Kobayashi, J. Normand, K. Raghavachari, A. Rendell, J. C. Burant, S. S. Iyengar, J. Tomasi, M. Cossi, J. M. Millam, M. Klene, C. Adamo, R. Cammi, J. W. Ochterski, R. L. Martin, K. Morokuma, O. Farkas, J. B. Foresman and D. J. Fox, *Gaussian 09, revision D.01*, Gaussian, Inc., Wallingford, CT, 2009.
- 30 A. Nakajima, *Bull. Chem. Soc. Jpn.*, 1971, **44**, 3272–3277.
- 31 (a) O. Narwark, S. Meskers, R. Peetz, E. Thorn-Csányi and H. Bässler, *Chem. Phys.*, 2003, **294**, 1–15; (b) J. Chen, E. Wuttke, W. Polit, T. Exner and R. F. Winter, *J. Am. Chem. Soc.*, 2013, **135**, 3391–3394.
- 32 S. Stoll and A. Schweiger, *J. Magn. Reson.*, 2006, **178**, 42–55.
- 33 S. Grimme, J. Antony, S. Ehrlich and H. Krieg, *J. Chem. Phys.*, 2010, **132**, 154104.
- 34 M. Cossi, N. Rega, G. Scalmani and V. Barone, *J. Comput. Chem.*, 2003, 669–681.
- 35 P. C. Hariharan and J. A. Pople, *Theor. Chim. Acta*, 1973, **28**, 213–222.
- 36 J. P. Perdew, K. Burke and M. Ernzerhof, *Phys. Rev. Lett.*, 1996, **77**, 3865–3868.
- 37 C. Adamo and V. Barone, *J. Chem. Phys.*, 1999, **110**, 6158–6170.
- 38 N. M. O’Boyle, A. L. Tenderholt and K. M. Langner, *J. Comput. Chem.*, 2008, **29**, 839–845.
- 39 M. D. Hanwell, D. E. Curtis, D. C. Lonie, T. Vandermeersch, E. Zurek and G. R. Hutchison, *J. Cheminf.*, 2012, 1–17.
- 40 O. Tange, *USENIX Mag.*, 2011, **36**, 42–47.
- 41 W. Humphrey, A. Dalke and K. Schulten, *J. Mol. Graphics*, 1996, **14**, 33–38.

